Supplement of Clim. Past, 19, 901–913, 2023
https://doi.org/10.5194/cp-19-901-2023-supplement

Climate of the Past
Open Access
EGU

Supplement of

Atlantic circulation changes across a stadial–interstadial transition

Claire Waelbroeck et al.

Correspondence to: Claire Waelbroeck (claire.waelbroeck@locean.ipsl.fr)

Supplement

The supplementary material includes:

- Supplementary text

Text S1. New *Cibicides* $\delta^{13}C$ records

Text S2. Dating of the 18 selected cores

Text S3. *Cibicides* $\delta^{13}C$ uncertainties

Text S4. Comparison between benthic $\delta^{18}O$ and simulated density changes

- Supplementary figures

Fig. S1. NorESM1-F simulated $\delta^{13}C$-BIO and observed *Cibicides* $\delta^{13}C$ time

Fig. S2. Linear regressions between calculated GI8-HS4 $\Delta\delta^{13}C$-BIO and observed GI8-HS4 Δ*Cib.* $\delta^{13}C$

Fig. S3. Dating information for cores MD03-2698 and CAR13-05

Fig. S4. Simulated AMOC and $\delta^{13}C$-BIO evolution versus age in calendar ky BP

Fig. S5. NorESM1-F simulated changes in preformed PO_4 at different water depths

Fig. S6. NorESM1-F simulated changes in PO_4 and Primary Production across the HS4-GI8 transition in the Atlantic euphotic layer

Fig. S7. % change in the simulated $\delta^{13}C$-BIO change across the HS4-GI8 transition

Fig. S8. Change in the simulated $\delta^{13}C$-BIO due to remineralization change, versus computed ideal age change

Fig. S9. Change in simulated $\delta^{13}C$-BIO across the HS4-GI8 transition at the 18 selected sites versus water depth

Fig. S10. NorESM1-F simulated changes in δ^{13}C-BIO and its partition into $(\Delta\delta^{13}\text{C-BIO})_{circ+PP}$ and $(\Delta\delta^{13}\text{C-BIO})_{rem}$ at different water depths

- Supplementary tables

Tab. S1. *Cibicides* δ^{13}C records references and dating information

Tab. S2. Observed and computed δ^{13}C during HS4, GI8, and corresponding changes across the HS4-GI8 transition

- References

Text S1. New *Cibicides* δ^{13}C records

Cibicides stable isotopes were measured in core CAR2013-PQP-CAR05 (abbreviated as CAR13-05), MD03-2698, MD13-3438, MD16-3511Q, SU90-08 and SU90-44 (Tab. S1), core MD16-3511Q having been collected in the Southern Ocean during the 2016 ACCLIMATE cruise (Waelbroeck and Michel, 2016). Epifaunal benthic foraminifers of the *Cibicides* genus were hand picked in the > 150 mm size fraction. *Cibicides wuellerstorfi* samples were picked when possible. However, in some levels of core CAR13-05, MD03-2698, SU90-08 and SU90-44, the only species present was *Cibicides kullenbergi*. When both species were present, we measured both and did not observe any significant difference in isotopic values between *Cibicides wuellerstorfi* and *Cibicides kullenbergi*. Similarly, in a few levels of core MD03-2698, *Cibicides sp.* was the only species present but we were able to verify that there was no isotopic offset with respect to *C. wuellerstorfi*. In each of these 6 cores, the measurements made on *Cibicides wuellerstorfi*, *Cibicides kullenbergi*, and *Cibicides* sp. were thus merged.

The samples were cleaned in a methanol ultrasonic bath during a few seconds. In the case of core SU90-08 which had been already studied at LSCE, the samples were further roasted under vacuum at 380 °C for 45 min prior to isotopic analyses (Duplessy, 1978) for the sake of consistency with previous measurements made on that core.

Cibicides $^{13}C/^{12}C$ ratios (δ^{13}C, expressed in ‰ versus VPDB) were measured at LSCE on an Isoprime100 mass-spectrometer on samples of 1 to 5 specimens. VPDB (Vienna PDB) is defined with respect to NBS19 calcite standard (δ^{18}O = 2.20% and δ^{13}C = +1.95%) (Coplen, 1988). The mean external reproducibility (1σ) of carbonate standards is ± 0.05 ‰ for δ^{18}O and ± 0.03 ‰ for δ^{13}C; measured NBS18 δ^{18}O is -23.27 ± 0.10 ‰VPDB and δ^{13}C is -5.01 ± 0.03 ‰VPDB.

Text S2. Dating of the 18 selected cores

The age models of the set of 92 cores published in (Waelbroeck et al., 2019) have been updated using IntCal20. The updated age models are available on the Seanoe data repository (https://www.seanoe.org/data/00484/59554/). 6 of the 18 cores selected in the present study are not included in the set of previously published age models because they are dated by a combination of direct chronological markers and alignment to one of the 92 previously dated core taken as a reference (Tab. S1).

- Core CAR13-05 is dated by a combination of radiocarbon dates, tie points defined by alignment of its % *Neogloboquadrina pachyderma*, a proxy of sea surface temperature (SST), to the NGRIP air temperature proxy record on the GICC05 age scale, and alignment of its IRD signal at the onset of HS4 HS3 and HS2 with the IRD signal of well-dated neighboring core SU92-03 taken as reference.

- Core KNR191-CDH19 is dated by alignment of its $CaCO_3$ XRF-signal to the $\%CaCO_3$ signal of well-dated core KNR31-GPC5 that was collected at the same site.

- The upper 7 m of core MD01-2444 are dated by alignment of its *Globigerina bulloides* $\delta^{18}O$ signal with that of well-dated neighboring core MD99-2334K. Below 7 m (i.e. for ages older than ~27 ka), core MD01-2444 is directly dated by alignment of its foraminiferal SST and *G. bulloides* $\delta^{18}O$ signals to the NGRIP temperature signal on the GICC05 age scale.

- Core SU90-44 is mainly dated by alignment of its *N. pachyderma* $\delta^{18}O$ and % *N. pachyderma* signals with the corresponding signals of well-dated neighboring core DSDP609. In addition to this alignment to core DSDP609, 1 alignment tie point is defined at 23.29 ± 0.30 ka by direct alignment of core SU90-44 % *N. pachyderma* signal to the NGRIP temperature on the GICC05 age scale.

- IODP core U1308 is mainly dated by alignment of its reflectance signal to that of core DSDP609, collected at the same site. Two additional tie points were defined by alignment of its Ca/Sr signal to DSDP609 IRD record.

- Core MD13-3438 was collected at the same site as core MD95-2002. It is dated by alignment of its Ti/Ca XRF signal to that of core MD95-2002 down to 14 m. Planktonic foraminifera census counts were produced on core MD13-3438 between 13.3 and 16.2 m. Therefore, core MD13-3438 could be dated by direct alignment of its % *N. pachyderma* and Ti/Ca XRF signals to NGRIP temperature and Ca^{++} signals respectively between 14 and 16.2 m. Finally, core MD13-3438 was dated by direct alignment of its Ti/Ca XRF signal to the NGRIP Ca^{++} signal below 16.2 m.

The dating files of these 6 additional cores are provided in the same format as that of the 92 age models published in (Waelbroeck et al., 2019) and can be downloaded from the Seanoe data repository (https://doi.org/10.17882/91130).

Finally, 4 previously published age models were improved with respect to their 2019 version. All updated age models are available on the Seanoe data repository (https://www.seanoe.org/data/00484/59554/), together with a readme file shortly describing the changes made. For the sake of completeness, here is a description of the changes made to the age models of the 4 cores involved in the present study.

- In core NA87-22, the tie points defined by alignment of its % *N. pachyderma* signal to NGRIP were revised before 34 ka in order to avoid unreasonably large surface reservoir ages.

- In core SU90-08, the largest of the two successive increases in the foraminiferal SST signal was chosen to define the tie point at end of HS4 through the alignment of the SST signal to the NGRIP temperature signal.

- In core MD99-2331, the tie points defined by alignment of its % *N. pachyderma* signal to NGRIP were revised around 25 ka in order to avoid unreasonably large surface reservoir ages.

- In MD03-2698, the tie points defined by alignment of its *G. bulloides* $\delta^{18}O$ signal to NGRIP were revised to account for the increased temporal resolution of the newly generated *G. bulloides* $\delta^{18}O$ record.

Text S3. *Cibicides* $\delta^{13}C$ uncertainties

We computed the 1 sigma uncertainty associated with the average HS4 and GI8 *Cib.* $\delta^{13}C$ values computed over the two 500 y intervals by combining the uncertainty resulting from the dispersion of the *Cib.* $\delta^{13}C$ measurements within each 500 y interval, and the dating uncertainties, assuming Gaussian error propagation.

Our marine core age models provide age uncertainty probability density functions and 68.27% and 95.45% dating confidence intervals for each data point along the cores (Waelbroeck et al., 2019;Lougheed and Obrochta, 2019). In order to account for dating uncertainties when estimate the uncertainty associated with the average HS4 and GI8 *Cib.* $\delta^{13}C$ values computed over the two 500 y intervals, we computed weighted averaged *Cib.* $\delta^{13}C$ values from all *Cib.* $\delta^{13}C$ measurements whose ages fully or partly intersect the 38.5-39.0 ka and 37.5-38.0 ka intervals. This way, data points with ages just outside the 38.5-39.0 ka and 37.5-38.0 ka intervals are accounted for, but with a smaller weight (<1) than the data points whose ages are comprised within the intervals, and their contribution decreases toward zero the farther away their dates are from the defined 38.5-39.0 ka and 37.5-38.0 ka intervals.

Text S4. Comparison between benthic $\delta^{18}O$ and simulated density changes

An increase in benthic $\delta^{18}O$ can be interpreted as an increase in bottom water density since it derives from either a decrease in bottom water temperature or an increase in bottom water $\delta^{18}O$ or salinity. It is thus interesting to compare the observed benthic $\delta^{18}O$ changes with the computed bottom water density changes. However, the change in benthic $\delta^{18}O$ across the HS4 to GI8 transition is unfortunately very small and not significant for most sites.

We have reported the changes in benthic $\delta^{18}O$ across the HS4 to GI8 transition in the table below. Note that we computed both *Cib.* $\delta^{18}O$ and $\delta^{18}O$ of mixed benthics when both data were available. We find significant benthic $\delta^{18}O$ changes across the HS4 to GI8 transition in only 5 North Atlantic sites. However, in core SU90-24, the 0.31 ± 0.15‰ decrease we compute based on the *Cib.* $\delta^{18}O$ record does not appear robust because we obtain no significant change (+0.13 ± 0.17‰) when combining (after due correction for species vital effects) *Cib.* $\delta^{18}O$ with the *Melonis pompilioides* $\delta^{18}O$ measurements available at higher resolution for that core.

In the remaining 4 sites, we find slight increases of about 0.2‰ in benthic $\delta^{18}O$ across the HS4 to GI8 transition for the 3 cores located between 2100 and 3100 m, and a 0.22 ± 0.16 ‰ decrease in core U1308 located at about 3900 m.

					HS4		GI8		HS4-GI8 amplitude					
Core	Species	Depth, m	Latitude (-90 to +90)	Longitude (-180 to +180)	Cib. d18O, ‰ PDB (38.5-39ka)	±, ‰	Cib. d18O, ‰ PDB (37.5-38ka)	±, ‰	GI8-HS4 Cib. d13C, ‰ PDB	±, ‰	GI8-HS4 computed d13C-BIO, ‰ PDB	±, ‰	GI8-HS4 Cib. d18O, ‰ PDB	±, ‰
SU90-24	CWU	**2085**	62.07	-37.03	3.90	0.10	3.59	0.11	**0.79**	0.16	**0.43**	0.02	**-0.31**	**0.15**
SU90-24	MXB	2085	62.07	-37.03	3.73	0.19	3.86	0.20					0.13	0.27
MD99-2331	CWU	2120	42.15	-9.68	3.61	0.10	3.48	0.14	**0.38**	**0.24**	**0.11**	0.01	-0.13	0.17
MD13-3438	CWU	2124	47.45	-8.45	3.46	0.15	3.63	0.19	**0.35**	**0.21**	**0.34**	0.01	0.17	0.24
NA87-22	CWU	**2161**	55.50	-14.70	3.75	0.10	3.97	0.20	**0.33**	0.20	**0.52**	0.01	**0.22**	**0.22**
GeoB3910	CWU	2344	-4.24	-36.35	3.60	0.16	3.59	0.13	**0.81**	0.23	**0.80**	0.02	-0.01	0.20
MD01-2444	CWU	2460	37.55	-10.13					**0.29**	0.25	**0.31**	0.02		
MD01-2444	MXB	**2460**	37.55	-10.13	2.93	0.12	3.12	0.12					**0.18**	**0.17**
MD95-2040	CIB	2465	40.58	-9.86	3.43	0.43	3.66	0.23	-0.04	0.46	**0.33**	0.01	0.23	0.49
SU90-08	CIB	**3080**	43.05	-30.04	3.44	0.10	3.69	0.11	**0.97**	**0.20**	**0.71**	0.01	**0.25**	**0.15**
MD95-2042	CIB	3146	37.80	-10.17	3.65	0.11	3.74	0.11	**0.61**	**0.17**	**0.15**	0.03	0.09	0.15
MD07-3076Q	CKU	3770	-44.15	-14.22	3.91	0.12	3.90	0.11	-0.13	0.28	**0.21**	0.01	-0.01	0.17
U1308	CIB	**3883**	49.88	-24.23	3.96	0.10	3.74	0.12	-0.09	0.33	0.01	0.06	**-0.22**	**0.16**
CH69-K09	CWU	4100	41.76	-47.35	3.64	0.19	3.70	0.19	**0.62**	**0.22**	**0.24**	0.05	0.06	0.27
SU90-44	CIB	4255	50.10	-17.91	3.74	0.22	3.87	0.15	0.24	0.28	**-0.05**	0.03	0.12	0.27
MD16-3511Q	CWU	4435	-35.36	29.24	3.98	0.11	4.02	0.10	**0.34**	**0.17**	**-0.06**	0.01	0.04	0.15
KNR191-CDH19	CIB	4541	33.69	-57.58	3.86	0.11	3.86	0.13	-0.03	0.24	-0.02	0.02	-0.01	0.17
MD03-2698	CIB	4602	38.24	-10.39	3.80	0.15	3.75	0.21	-0.03	0.29	**-0.07**	0.04	-0.05	0.26
CAR13-05	CIB	4870	45.00	-14.33	3.73	0.15	3.75	0.19	**0.36**	**0.28**	**-0.12**	0.06	0.03	0.24
TNO57-21	CWU	4981	-41.10	7.80	4.00	0.11	3.96	0.10	-0.07	0.28	**-0.12**	0.04	-0.04	0.15

in bold: significant changes

Importantly, the modern relationship between bottom water $\delta^{18}O$ and salinity does not hold in glacial periods due to the large changes in the hydrological cycle between the glacial and modern climate. Therefore, benthic $\delta^{18}O$ and bottom water density changes across the HS4 to GI8 transition can only be qualitatively compared.

The figure below shows the computed bottom water density, temperature and salinity at the 4 sites where we find significant changes in benthic $\delta^{18}O$. Unfortunately, in contrast to the computed $\delta^{13}C$-BIO (see Fig. S1), the computed bottom water density and temperature do not reach relatively stable values in the three upper sites at the end of the fresh water forcing (FWF), but are still steadily changing. The bottom water density at these three sites is steadily decreasing, while the bottom water temperature is steadily increasing, at rates that appear approximately constant over the second half of the FWF interval. Therefore, it is very likely that the computed bottom water density and temperature would reach lower and higher values respectively, had the FWF been maintained for another 900 y to attain the total 1700 y duration of Heinrich 4 stadial. However, this is somewhat speculative and we cannot draw firm conclusions regarding the sign of the simulated change in density at the three upper sites.

In the deepest site (U1308), bottom water density, temperature and salinity have reach relatively stable values before the end of the FWF. The simulated change in bottom water density across the HS4 to GI8 transition is a small decrease, in agreement with the 0.22 ± 0.16 ‰ decrease in benthic $\delta^{18}O$ found at that site. This model-data agreement thus validates the simulated change in bottom water properties across the HS4 to GI8 transition at site U1308.

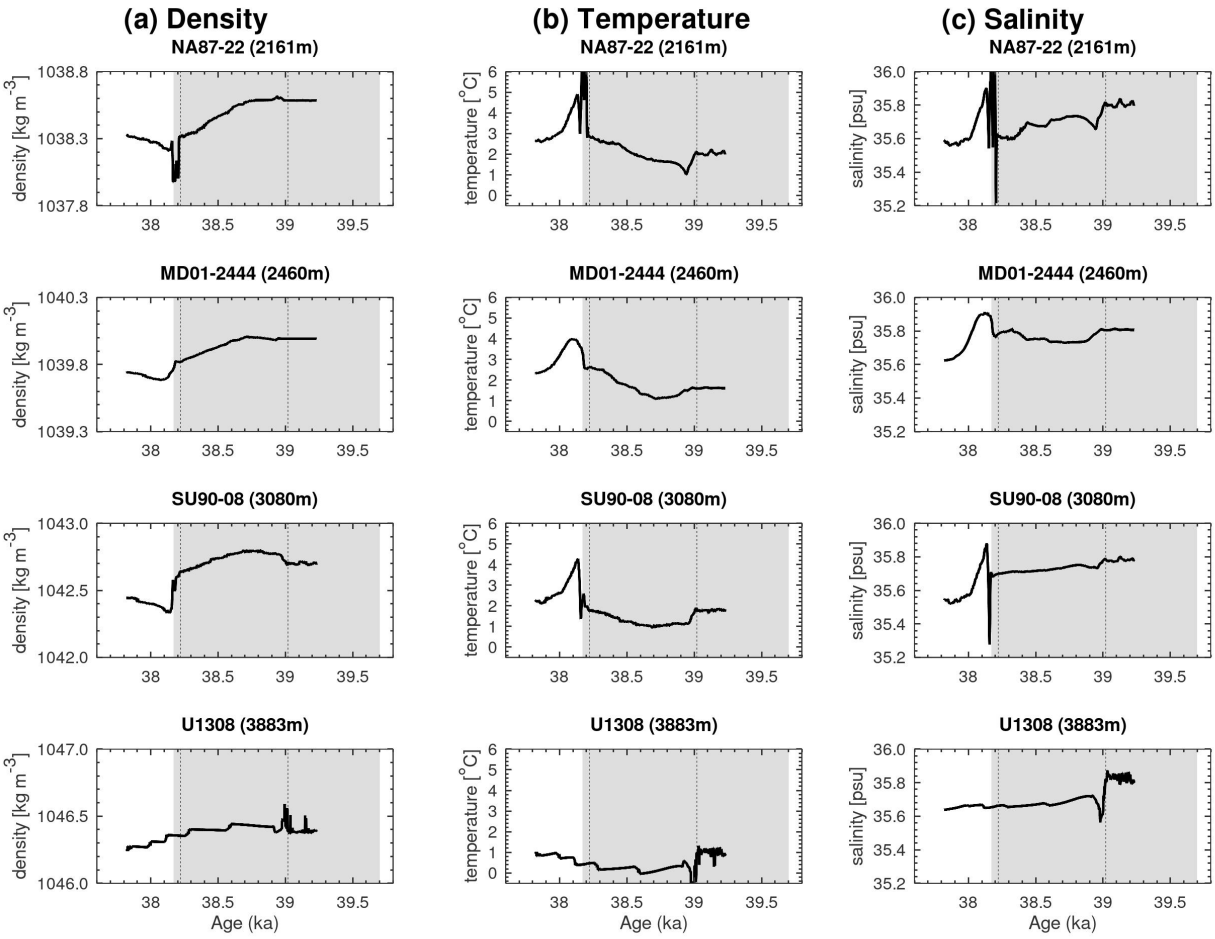

Figure caption: Simulated bottom water density **(a)**, temperature **(b),** and salinity **(c)** versus age in calendar ky BP across the HS4 to GI8 transition. The grey band denotes the HS4 time interval. The dotted vertical lines indicate the beginning and end of the 800 y long freshwater flux hosing experiment. Model years have been shifted so that the mid-slope of the stadial-interstadial transition takes place at end of Heinrich stadial 4 (i.e. at 38.17 ka) as in Fig. S4.

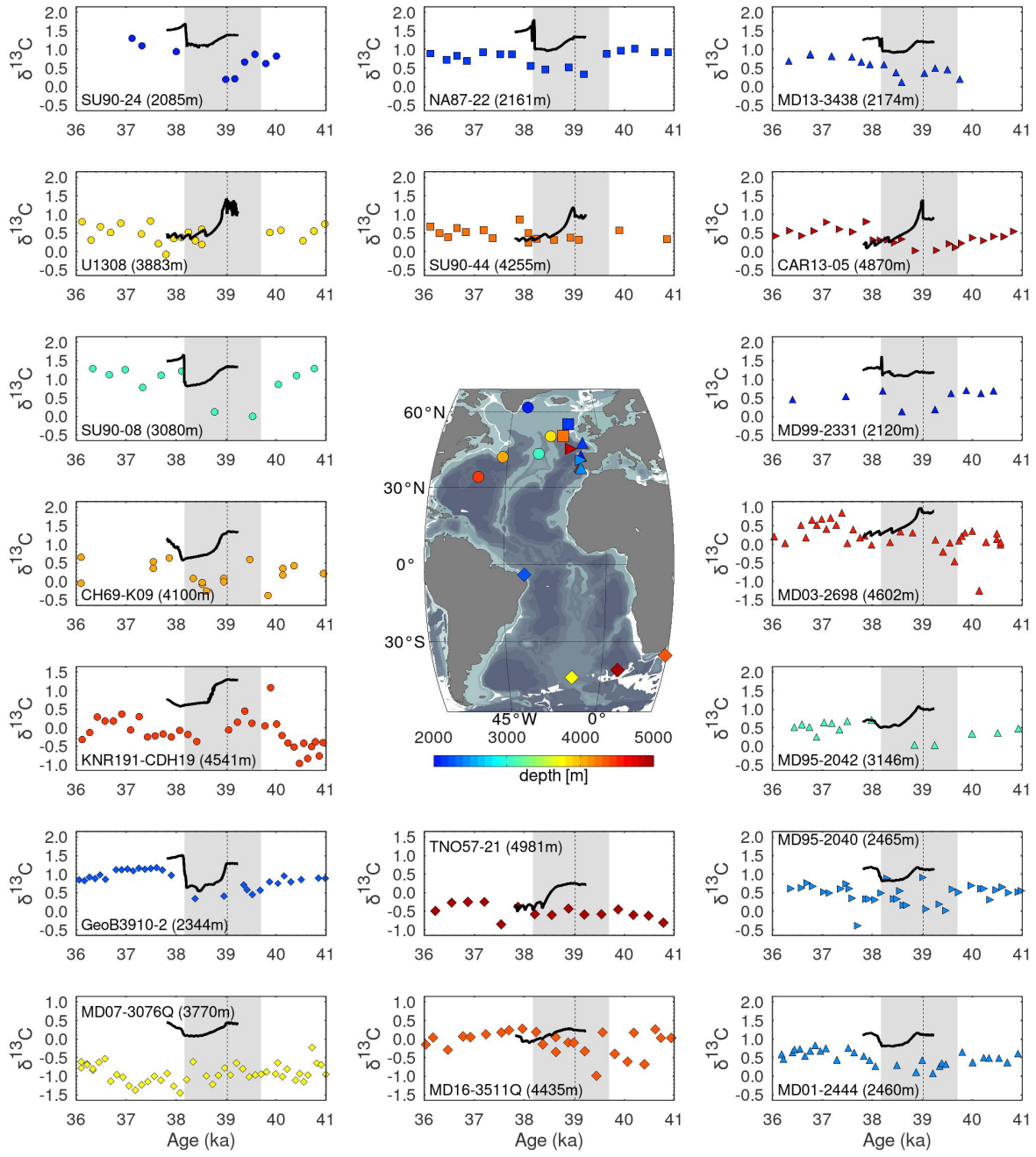

Fig. S1. NorESM1-F simulated δ^{13}C-BIO (black curve) and observed *Cibicides* δ^{13}C (symbols) time series over the 36-41 ka time interval at the 18 selected sites. Full coordinates of the sites are given in Tab. 1. The grey band corresponds to the Heinrich stadial 4 chronozone. The dotted vertical line indicates the beginning of the freshwater flux input (see Fig. S4).

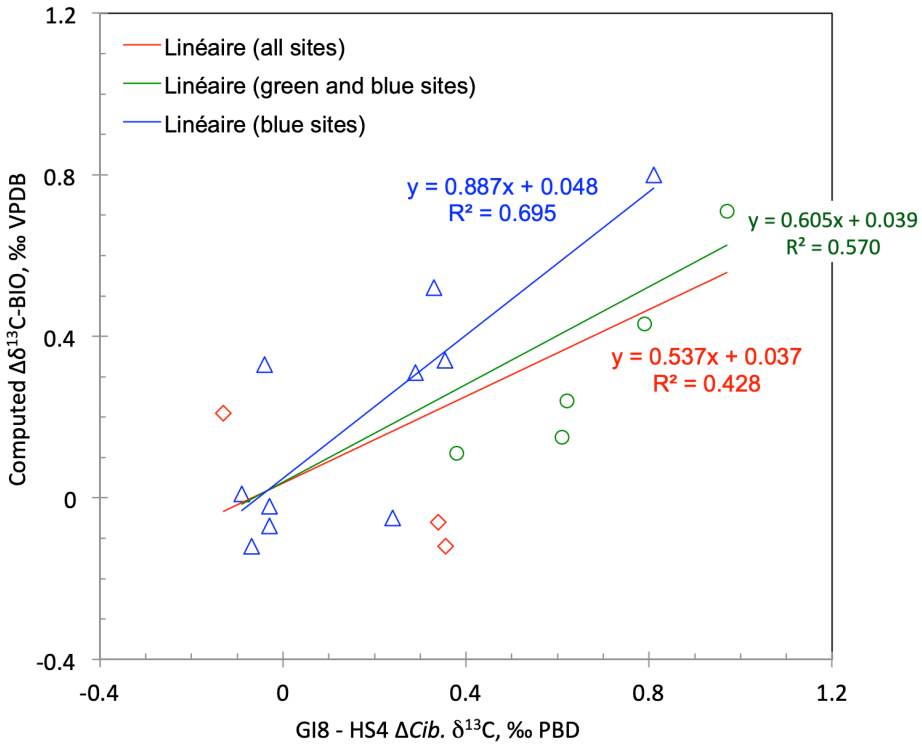

Fig. S2. Linear regressions between calculated GI8-HS4 $\Delta\delta^{13}$C-BIO and observed GI8-HS4 Δ*Cib.* δ^{13}C for (i) all sites (red line, n=18), (ii) only sites depicted in blue and green, i.e., strict model-data agreement + agreement between simulated and observed trends (green line, n=15), and (iii) only blue sites, i.e., strict model-data agreement (blue line, n=10). Probabilities of no linear correlation = 0.006, 0.003 and 0.007, for the red, green and blue regression lines respectively.

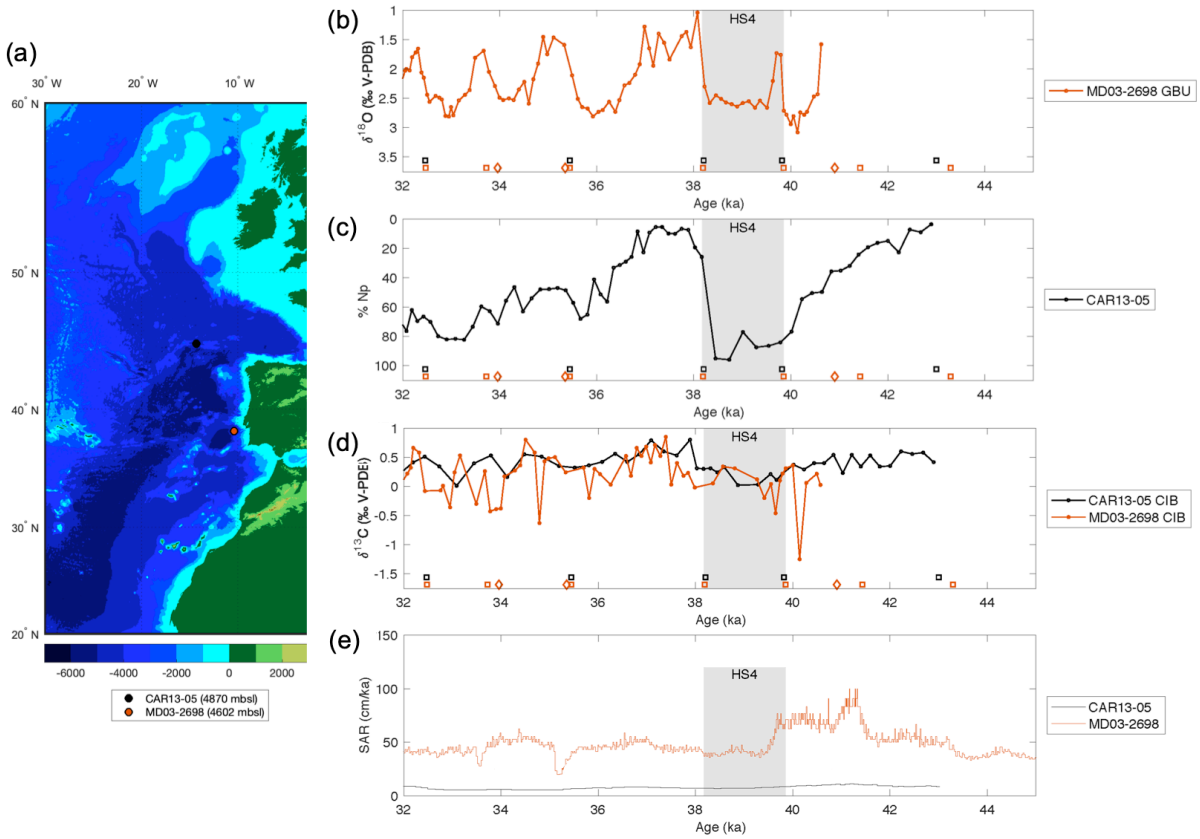

Fig. S3. Dating information for cores MD03-2698 and CAR13-05 over 32-45 ka. **(a)** Location of the 2 cores. **(b)** MD03-2698 *G. bulloides* $\delta^{18}O$ record (ACCLIMATE data), a proxy for SST on the Iberian margin. **(c)** CAR13-05 % *N. pachyderma* (ACCLIMATE data), a proxy for SST. **(d)** *Cibicides* $\delta^{13}C$ records of both cores. **(e)** Sediment accumulation rates of both cores. Diamonds and squares above the X-axis in panels **b-d** denote radiocarbon dates and alignment pointers, respectively (Waelbroeck et al., 2019). Plots made with the PARIS software (Lougheed et al., 2022).

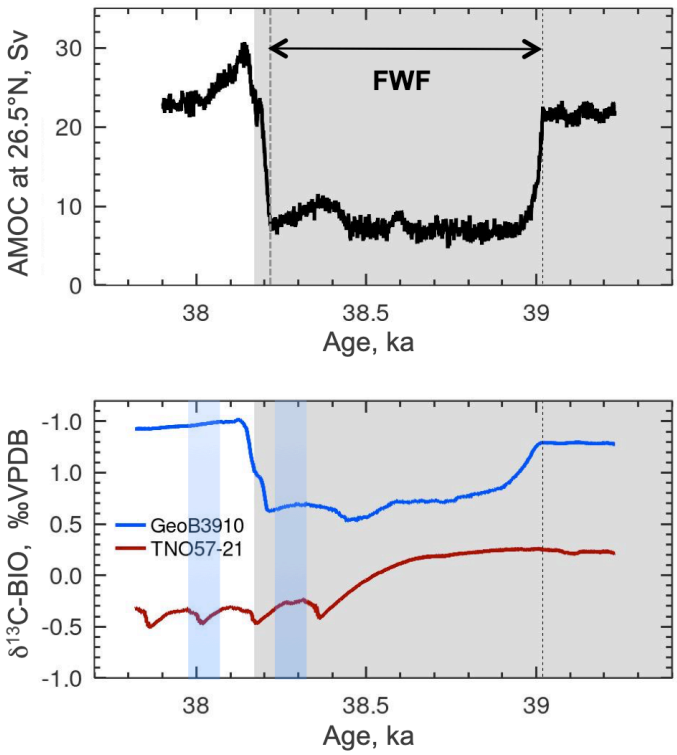

Fig. S4. Simulated AMOC and δ^{13}C-BIO evolution versus age in calendar ky BP. **Upper panel**: simulated maximum North Atlantic meridional stream function at 26.5°N. The dotted vertical lines indicate the beginning and end of the 800 y long freshwater flux hosing experiment. Model years have been shifted so that the midslope of the stadial-interstadial transition takes place at end of Heinrich stadial 4 (i.e. at 38.17 ka). **Lower panel**: simulated δ^{13}C-BIO at two core sites, as represented in Fig. S1. The grey band highlights the portion of the represented time interval belonging to HS4; the blue bands highlight the pre and post-transition 100 y intervals over which model results are averaged.

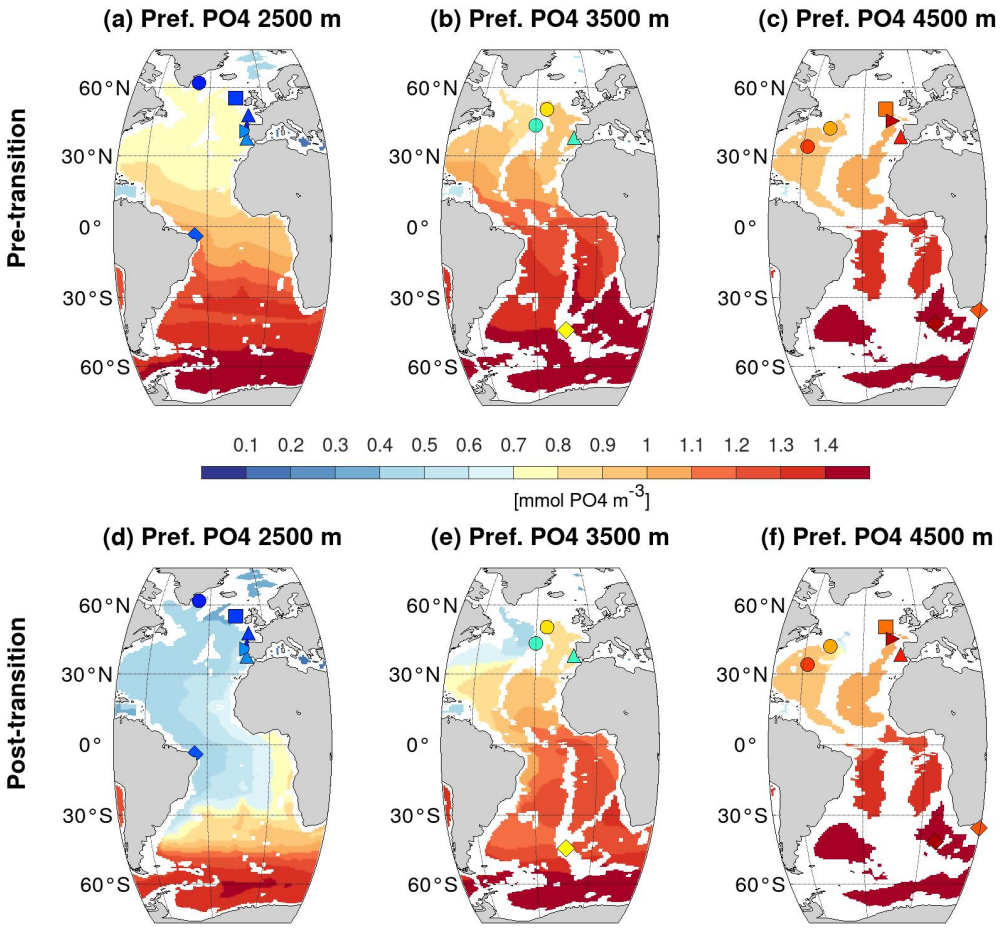

Fig. S5. NorESM1-F simulated changes in preformed PO_4 at 2500, 3500 and 4500 m depth in the Atlantic Ocean across the HS4-GI8 transition. Pre- and post-transition values correspond to 100 y averages over model year Y 5700-5800 of the "fw-on" run, and Y 5950-6050 of the "fw-off" run, respectively.

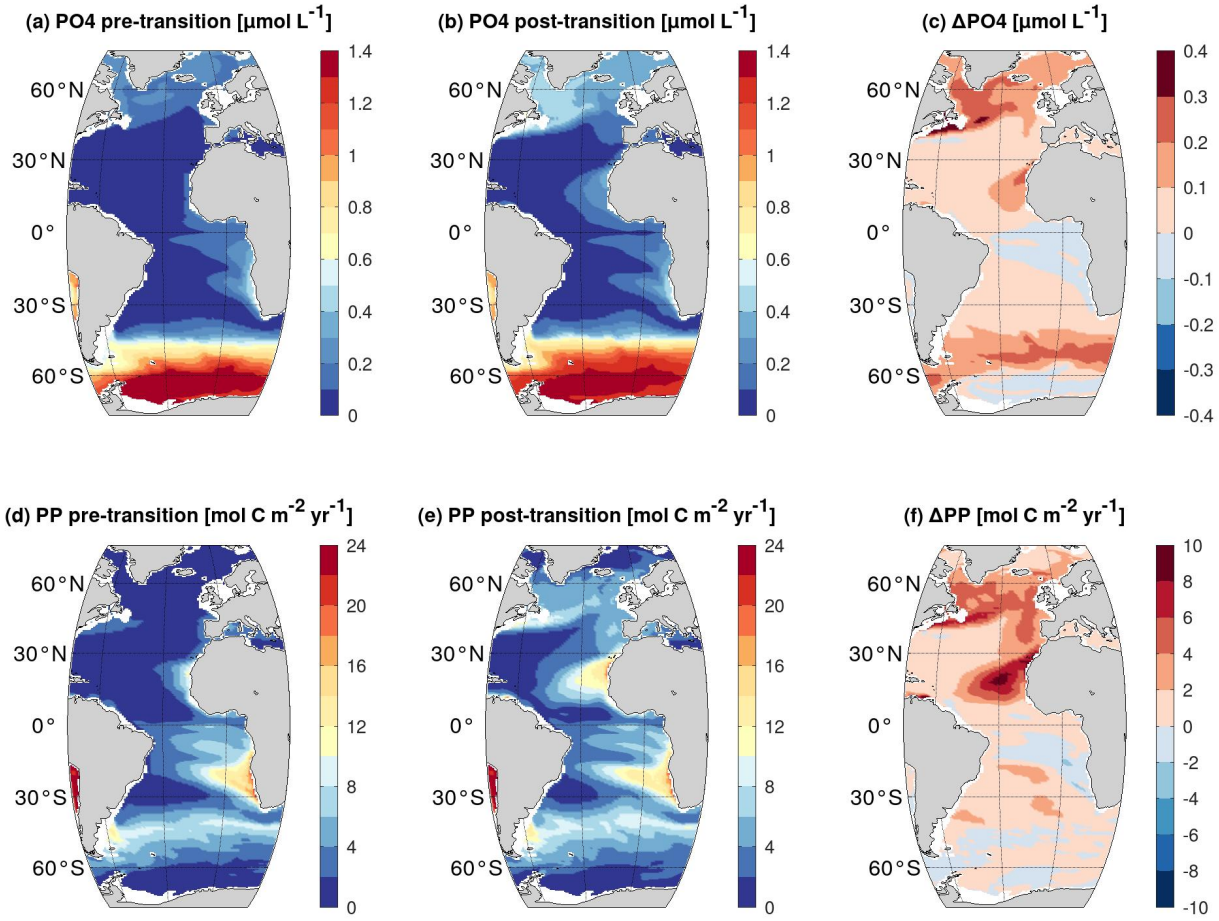

Fig. S6. NorESM1-F simulated changes in PO_4 and Primary Production across the HS4-GI8 transition in the Atlantic euphotic layer. **(a)-(c)** Simulated PO4 in the upper 100 m. **(d)-(f)** Simulated PP in the euphotic layer (upper 112.5 m). Pre- and post-transition values correspond to 100 y averages over model year Y 5700-5800 of the "fw-on" run, and Y 5950-6050 of the "fw-off" run, respectively.

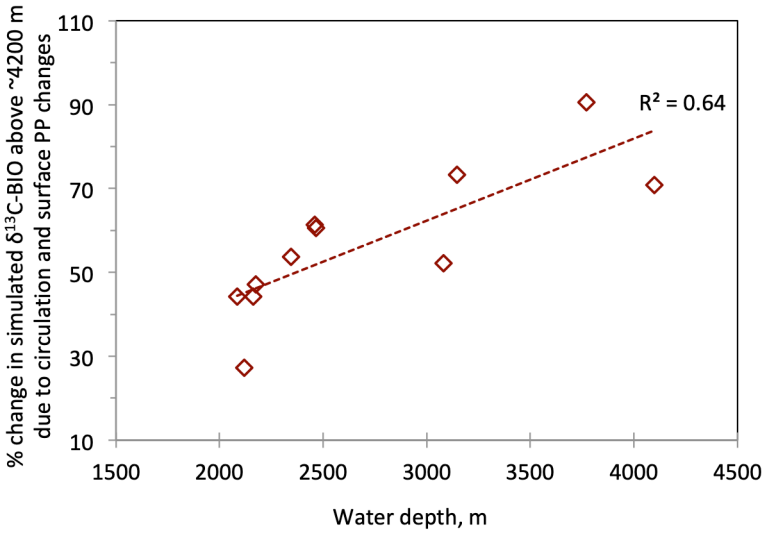

Fig. S7. % change in the simulated δ^{13}C-BIO change across the HS4-GI8 transition due to ocean circulation and surface PP changes in the 11 sites located above 4200 m which exhibit significant GI8-HS4 δ^{13}C-BIO changes

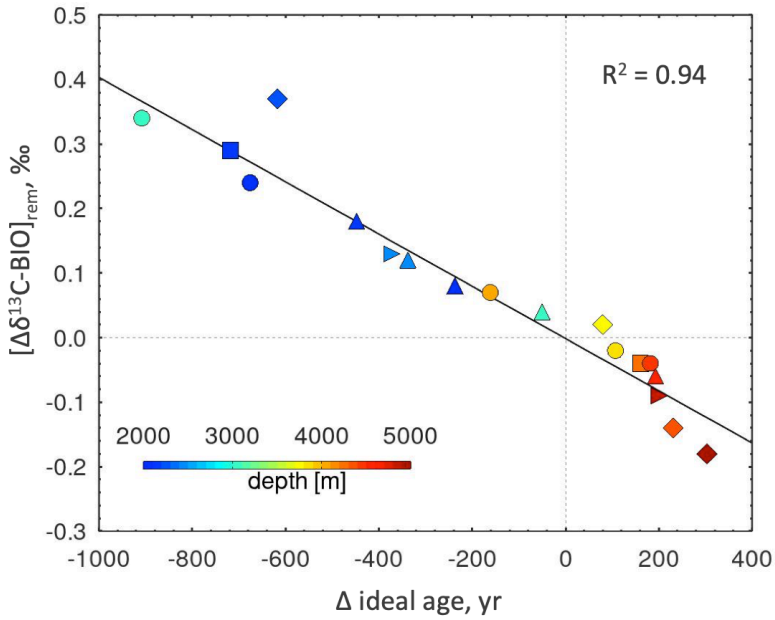

Fig. S8. Change in the simulated δ^{13}C-BIO due to remineralization change, versus computed ideal age change across the HS4-GI8 transition at each core site. Symbols as in Fig. S1.

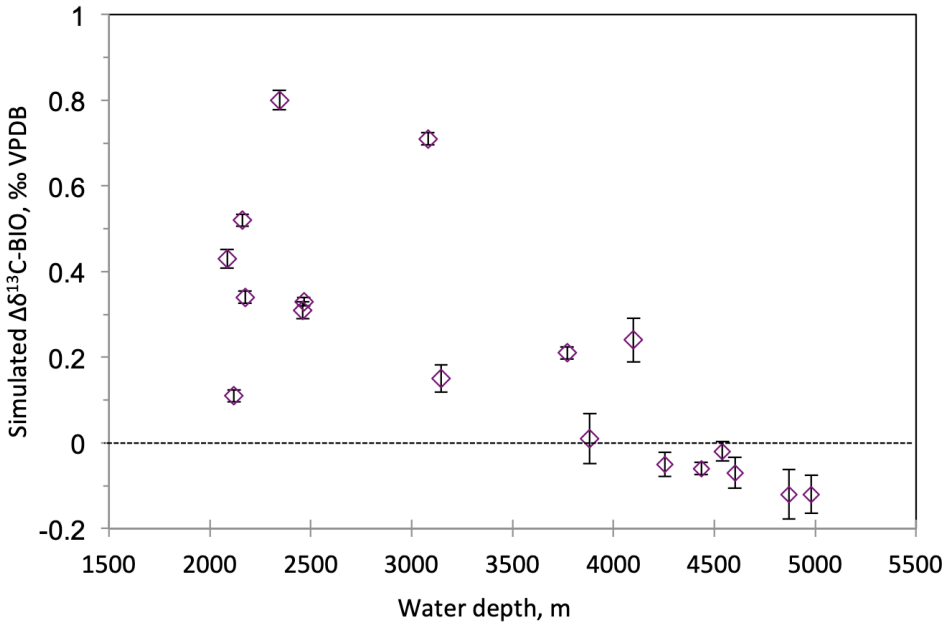

Fig. S9. Change in simulated δ^{13}C-BIO across the HS4-GI8 transition at the 18 selected sites versus water depth.

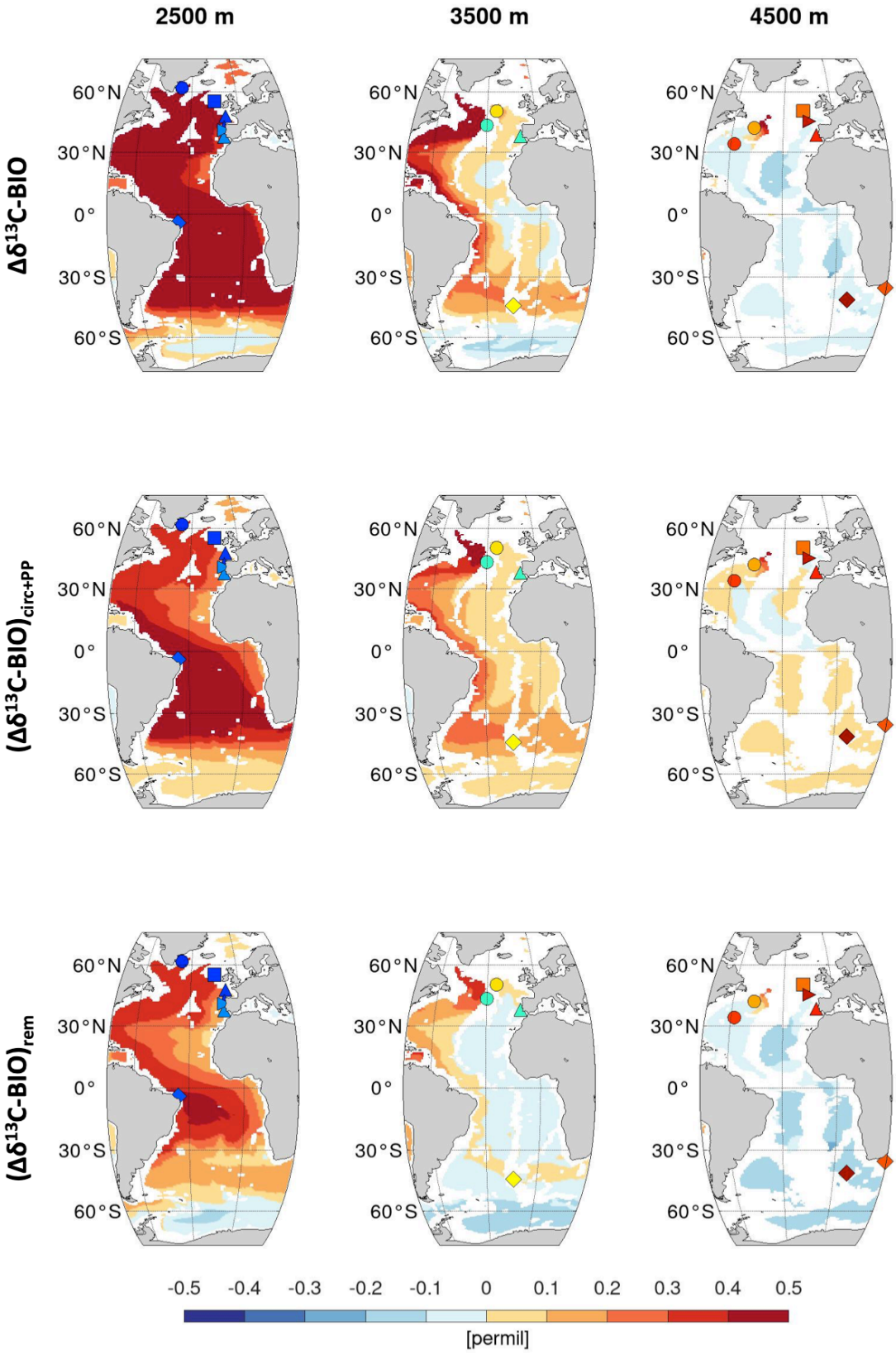

Fig. S10. NorESM1-F simulated changes in δ^{13}C-BIO and its partition into $(\Delta\delta^{13}\text{C-BIO})_{\text{circ+PP}}$ and $(\Delta\delta^{13}\text{C-BIO})_{\text{rem}}$ at 2500, 3500 and 4500 m depth in the Atlantic Ocean across the HS4-GI8 transition.

Table S1. *Cibicides* $\delta^{13}C$ records references and dating information

Core	Species	Depth, m	Latitude, decimals	Longitude, decimals	*Cibicides* $\delta^{13}C$ references	Dating
SU90-24	CWU	2085	62.07	-37.03	[*Elliot et al.*, 2002]	[*Waelbroeck et al.*, 2019]
NA87-22	CWU	2161	55.50	-14.70	[Vidal et al., 1997]	[*Waelbroeck et al.*, 2019] improved
SU90-44	CIB	4255	50.10	-17.91	ACCLIMATE data	this study
U1308	CIB	3883	49.88	-24.23	[*Hodell and Channell*, 2016]	this study
MD13-3438	CWU	2124	47.45	-8.45	ACCLIMATE data	this study
CAR13-05	CIB	4870	45.00	-14.33	ACCLIMATE data	this study
SU90-08	CIB	3080	43.05	-30.04	ACCLIMATE data	[*Waelbroeck et al.*, 2019] improved
MD99-2331	CWU	2120	42.15	-9.68	LSCE unpublished data	[*Waelbroeck et al.*, 2019] improved
CH69-K09	CWU	4100	41.76	-47.35	[*Labeyrie et al.*, 1999]	[*Waelbroeck et al.*, 2019]
MD95-2040	CIB	2465	40.58	-9.86	[*Voelker and de Abreu*, 2011]	[*Waelbroeck et al.*, 2019]
MD03-2698	CIB	4602	38.24	-10.39	ACCLIMATE data	[*Waelbroeck et al.*, 2019] improved
MD95-2042	CIB	3146	37.80	-10.17	[*Shackleton et al.*, 2000]	[*Waelbroeck et al.*, 2019]
MD01-2444	CWU	2460	37.55	-10.13	[Skinner et al., 2007]	this study
KNR191-CDH19	CIB	4541	33.69	-57.58	[Henry et al., 2016]	this study
GeoB3910	CWU	2344	-4.24	-36.35	[*Burckel et al.*, 2015]	[*Waelbroeck et al.*, 2019]
MD16-3511Q	CWU	4435	-35.36	29.24	ACCLIMATE data	[*Waelbroeck et al.*, 2019]
TNO57-21	CWU	4981	-41.10	7.80	[*Ninnemann et al.*, 1999; *Barker and Diz*, 2014]	[*Waelbroeck et al.*, 2019]
MD07-3076Q	CKU	3770	-44.15	-14.22	[*Gottschalk et al.*, 2016]	[*Waelbroeck et al.*, 2019]

Tab. S1. *Cibicides* $\delta^{13}C$ records references and dating information.

Table S2. Observed and computed $\delta^{13}C$ during HS4, GI8, and corresponding changes across the HS4-GI8 transition

				HS4				GI8				HS4-GI8 amplitude			
						Computed				Computed					
Core	Depth, m	Latitude, decimals	Longitude, decimals	*Cib.* $\delta^{13}C$, ‰ VPDB	± 1σ, ‰	$\delta^{13}C$-BIO, ‰ VPDB	± 1σ, ‰	*Cib.* $\delta^{13}C$, ‰ VPDB	± 1σ, ‰	$\delta^{13}C$-BIO, ‰ VPDB	± 1σ, ‰	Δ*Cib.* $\delta^{13}C$, ‰	± 1σ, ‰	$\Delta\delta^{13}C$-BIO, ‰	± 1σ, ‰
SU90-24	2085	62.07	-37.03	0.20	0.10	1.14	0.02	0.99	0.12	1.57	0.01	**0.79**	0.16	**0.43**	0.02
NA87-22	2161	55.50	-14.70	0.48	0.12	1.01	0.01	0.81	0.16	1.53	0.01	**0.33**	0.20	**0.52**	0.01
SU90-44	4255	50.10	-17.91	0.34	0.10	0.37	0.02	0.58	0.26	0.32	0.02	0.24	0.28	**-0.05**	0.03
U1308	3883	49.88	-24.23	0.37	0.11	0.40	0.05	0.28	0.31	0.41	0.03	-0.09	0.33	0.01	0.06
MD13-3438	2180	47.45	-8.45	0.29	0.17	0.96	0.01	0.65	0.12	1.30	0.01	**0.35**	**0.21**	**0.34**	0.01
CAR13-05	4870	45.00	-14.33	0.19	0.17	0.35	0.03	0.55	0.22	0.23	0.05	**0.36**	**0.28**	**-0.12**	0.06
SU90-08	3080	43.05	-30.04	0.12	0.10	0.83	0.01	1.09	0.17	1.54	0.01	**0.97**	**0.20**	**0.71**	0.01
MD99-2331	2120	42.15	-9.68	0.21	0.21	1.19	0.01	0.59	0.12	1.30	0.01	**0.38**	**0.24**	**0.11**	0.01
CH69-K09	4100	41.76	-47.35	-0.08	0.17	0.64	0.01	0.54	0.14	0.88	0.05	**0.62**	**0.22**	**0.24**	0.05
MD95-2040	2465	40.58	-9.86	0.39	0.30	0.83	0.00	0.35	0.35	1.16	0.01	-0.04	0.46	**0.33**	0.01
MD03-2698	4602	38.24	-10.39	0.28	0.14	0.35	0.02	0.25	0.25	0.28	0.03	-0.03	0.29	**-0.07**	0.04
MD95-2042	3146	37.80	-10.17	0.04	0.10	0.52	0.01	0.65	0.14	0.67	0.03	**0.61**	**0.17**	**0.15**	0.03
MD01-2444	2460	37.55	-10.13	0.25	0.17	0.82	0.00	0.54	0.18	1.13	0.02	**0.29**	0.25	**0.31**	0.02
KNR191-CDH19	4541	33.69	-57.58	-0.16	0.21	0.63	0.01	-0.19	0.12	0.61	0.02	-0.03	0.24	-0.02	0.02
GeoB3910	2344	-4.24	-36.35	0.24	0.16	0.68	0.02	1.05	0.17	1.48	0.01	**0.81**	0.23	**0.80**	0.02
MD16-3511Q	4435	-35.36	29.24	-0.12	0.13	0.01	0.01	0.22	0.11	-0.05	0.01	**0.34**	**0.17**	**-0.06**	0.01
TNO57-21	4981	-41.10	7.80	-0.51	0.13	-0.27	0.02	-0.58	0.25	-0.39	0.04	-0.07	0.28	**-0.12**	0.04
MD07-3076Q	3770	-44.15	-14.22	-0.99	0.20	0.09	0.01	-1.12	0.19	0.30	0.01	-0.13	0.28	**0.21**	0.01

in green: good trend, but computed GI8-HS4 d13C-BIO smaller than the observed amplitude
in red: model-data disagreement
in bold: significant changes

Tab. S2. Observed and computed $\delta^{13}C$ during HS4, GI8, and corresponding changes across the HS4-GI8 transition.

References

Barker, S., and Diz, P.: Timing of the descent into the last Ice Age determined by the bipolar seesaw, Paleoceanography, 29, 489-507, 2014.

Burckel, P., Waelbroeck, C., Gherardi, J.-M., Pichat, S., Arz, H., Lippold, J., Dokken, T., and Thil, F.: Atlantic Ocean circulation changes preceded millennial tropical South America rainfall events during the last glacial, Geophys. Res. Lett., 42, 411-418, 10.1002/2014GL062512, 2015.

Coplen, T. B.: Normalization of oxygen and hydrogen isotope data, Chem. Geol., 72, 293-297, 1988.

Duplessy, J. C.: Isotope studies, in: Climatic changes, edited by: Gribbin, J., Cambridge University Press, Cambridge, 46- 67, 1978.

Elliot, M., Labeyrie, L., and Duplessy, J. C.: Changes in North-Atlantic deep-water formation associated with the Dansgaard-Oeschger temperature oscillations (60-10 ka), Quaternary Science Reviews, 21, 1153-1165, 2002.
Gottschalk, J., Skinner, L. C., Lippold, J., Vogel, H., Frank, N., Jaccard, S. L., and Waelbroeck, C.: Biological and physical controls in the Southern Ocean on past millennial-scale atmospheric CO2 changes, Nat Commun, 7, 10.1038/ncomms11539, 2016.
Henry, L., McManus, J. F., Curry, W. B., Roberts, N. L., Piotrowski, A. M., and Keigwin, L. D.: North Atlantic ocean circulation and abrupt climate change during the last glaciation, Science, 353, 470-474, 10.1126/science.aaf5529, 2016.
Hodell, D. A., and Channell, J. E.: Mode transitions in Northern Hemisphere glaciation: co-evolution of millennial and orbital variability in Quaternary climate, Climate of the Past, 12, 1805-1828, 2016.
Labeyrie, L., Leclaire, H., Waelbroeck, C., Cortijo, E., Duplessy, J.-C., Vidal, L., Elliot, M., and Lecoat, B.: Temporal Variability of the Surface and Deep Waters of the North West Atlantic Ocean at Orbital and Millennial scales, in: Geophysical Monograph Series 112, Mechanisms of global climate change at millennial time scales, edited by: Clark, P., Webb, R. S., and Keigwin, L. D., AGU, Washington, D.C., 77-98, 1999.
Lougheed, B. C., Waelbroeck, C., Smialkowski, N., Vazquez Riveiros, N., and Obrochta, S. P.: A Simplified Palaeoceanography Archiving System (PARIS) and GUI for Storage and Visualisation of Marine Sediment Core Proxy Data vs Age and Depth, Open Quaternary, 8, 1-11, 10.5334/oq.101, 2022.
Ninnemann, U. S., Charles, C. D., and Hodell, D. A.: Origin of global millennial scale climate events: Constraints from the Southern Ocean deep sea sedimentary record, in: Mechanisms of global climate change at millennial timescales, edited by: Clark, P. U., Webb, R. S., and Keigwin, L. D., Geophysical Monograph Series, American Geophysical Union, Washinton, D.C., 99-112, 1999.
Shackleton, N. J., Hall, M. A., and Vinent, E.: Phase relationships between millenial-scale events 64 000 - 24 000 years ago, Paleoceanography, 15, 565-569, 2000.
Skinner, L., Elderfield, H., and Hall, M.: Phasing of millennial climate events and Northeast Atlantic deep-water temperature change since 50 ka BP, in, Geophysical Monograph Series, 173, AGU, Washington, D.C., 197, 2007.
Vidal, L., Labeyrie, L., Cortijo, E., Arnold, M., Duplessy, J. C., Michel, E., Becqué, S., and van Weering, T. C. E.: Evidence for changes in the North Atlantic Deep Water linked to meltwater surges during the Heinrich events, Earth and Planetary Science Letters, 146, 13-26, 1997.
Voelker, A. H. L., and de Abreu, L.: A review of abrupt climate change events in the Northeastern Atlantic Ocean (Iberian Margin): Latitudinal, longitudinal, and vertical gradients, Geophysical Monograph Series, 193, 15-37, 2011.
Waelbroeck, C., and Michel, E.: ACCLIMATE-MD203 cruise report, Brest, 2016.
Waelbroeck, C., Lougheed, B. C., Vazquez Riveiros, N., Missiaen, L., Pedro, J., Dokken, T., Hajdas, I., Wacker, L., Abbott, P., Dumoulin, J.-P., Thil, F., Eynaud, F., Rossignol, L., Fersi, W., Albuquerque, A. L., Arz, H., Austin, W. E. N., Came, R., Carlson, A. E., Collins, J. A., Dennielou, B., Desprat, S., Dickson, A., Elliot, M., Farmer, C., Giraudeau, J., Gottschalk, J., Henderiks, J., Hughen, K., Jung, S., Knutz, P., Lebreiro, S., Lund, D. C., Lynch-Stieglitz, J., Malaizé, B., Marchitto, T., Martínez-Méndez, G., Mollenhauer, G., Naughton, F., Nave, S., Nürnberg, D., Oppo, D., Peck, V., Peeters, F. J. C., Penaud, A., Portilho-Ramos, R. d. C., Repschläger, J., Roberts, J., Rühlemann, C., Salgueiro, E., Sanchez Goni, M. F., Schönfeld, J., Scussolini, P., Skinner, L. C., Skonieczny, C., Thornalley, D., Toucanne, S., Rooij, D. V., Vidal, L., Voelker, A. H. L., Wary, M., Weldeab, S., and Ziegler, M.: Consistently dated Atlantic sediment cores over the last 40 thousand years, Scientific Data, 6, 165, 10.1038/s41597-019-0173-8, 2019.